INSTITUTE OF PHYSICS PUBLISHING JOURNAL OF OPTICS A: PURE AND APPLIED OPTICS

J. Opt. A: Pure Appl. Opt. **7** (2005) S12–S22 doi:10.1088/1464-4258/7/2/002

Left-handed metamaterials: detailed numerical studies of the transmission properties

M Kafesaki[1], Th Koschny[1], R S Penciu[1], T F Gundogdu[1], E N Economou[1,2] and C M Soukoulis[3,4,5]

[1] Institute of Electronic Structure and Laser (IESL), Foundation for Research and Technology Hellas (FORTH), PO Box 1527, 71110 Heraklion, Crete, Greece
[2] Department of Physics, University of Crete, Greece
[3] IESL-FORTH and Department of Materials Science and Technology, 71110 Heraklion, Crete, Greece
[4] Ames Laboratory and Department of Physics and Astronomy, Iowa State University, Ames, IA 50011, USA

E-mail: soukoulis@ameslab.gov

Received 13 July 2004, accepted for publication 30 September 2004
Published 20 January 2005
Online at stacks.iop.org/JOptA/7/S12

Abstract
Using numerical simulation techniques such as the transfer matrix method and the commercially available code Microwave Studio, we study the transmission properties of left-handed (LH) metamaterials and arrays of split-ring resonators (SRRs). We examine the dependence of the transmission through single- and double-ring SRRs on parameters of the system such as the size and shape of the SRRs, size of the unit cell, dielectric properties of the embedding medium where the SRRs reside, and SRR orientation relative to the incoming electromagnetic field. Moreover, we discuss the role of SRRs and wires on the electric cut-off frequency of the combined system of wires and SRRs, as well as the influence of the various system parameters on the LH transmission peak of a medium composed of SRRs and wires. Finally, demonstrating the disadvantages of the currently used SRR designs due to the lack of symmetry, we discuss more symmetric, multigap SRRs, which constitute very promising components for future two-dimensional and three-dimensional LH structures.

Keywords: left-handed materials, negative refraction, electromagnetic waves

(Some figures in this article are in colour only in the electronic version)

1. Introduction

Recently, there have been many studies of metamaterials that have a negative refractive index n. These materials, called left-handed materials (LHMs), theoretically discussed first by Veselago [1], have simultaneously negative electrical permittivity, ϵ, and magnetic permeability, μ. The first realization of such materials, consisting of split-ring resonators (SRRs) and continuous wires, was first introduced by Pendry [2, 3], who suggested that they can also act as perfect lenses [4].

The first experimental materialization of Pendry's ideas was made by Smith *et al* in 2000 [5], and since then various new samples have been prepared [6, 7] (composed of SRRs and wires), all of which have been shown to exhibit a pass band in which it was assumed that ϵ and μ are both negative.

This assumption was based on measuring independently the transmission, T, of the wires alone, and then T for the SRRs alone. If the peak in the combined metamaterial composed of SRRs and wires lay in the stop band for the SRRs alone (which

[5] Author to whom any correspondence should be addressed.

corresponds to negative μ) or that for the wires alone (which is thought to correspond to negative ϵ) the peak was considered to be left-handed (LH). Further support for this interpretation was provided by the demonstration that some of these materials exhibit negative refraction of electromagnetic waves [8].

Subsequent experiments [9] have reaffirmed the property of negative refraction, giving strong support to the interpretation that these metamaterials can be correctly described in terms of negative permeability, due to the SRRs, and negative permittivity, due to the wires. However, as was shown in [10], this is not always the case, as the SRRs also exhibit a resonant electric response, in addition to their magnetic response which was first described by Pendry [3]. The electric response of the SRRs, which is demonstrated by closing their air gaps (destroying therefore their magnetic response), is identical to that of cut wires, and it is added to the electric response (ϵ) of the wires. The result is that the effective plasma frequency, $\omega_{\rm p}'$, of the combined system of wires and SRRs (or closed SRRs) is always lower than the plasma frequency of just the wires, $\omega_{\rm p}$. With this consideration and the analytical expressions for ϵ and μ [10] which stem from it, one is able to reproduce all the low frequency transmission, T, and reflection, R, characteristics of LHMs. Even the minor details in T and R observed in the simulations can be analytically explained.

Moreover, the interpretation of [10] gave an easy criterion for identifying whether an experimental transmission peak is LH or right-handed (RH): if the closing of the gaps of the SRRs in a given LHM structure removes the peak close to the position of the SRR dip from the T spectrum, this is strong evidence that the T peak is indeed left-handed. If the gap above the peak is removed, the peak is most probably right-handed. This criterion is very valuable in experimental studies, where one cannot easily obtain the effective ϵ and μ. The criterion is used experimentally and it is found that some T peaks that were thought to be LH turn out to be RH [11].

There is also a significant amount of numerical work [12–17] in which the complex transmission and reflection amplitudes are calculated for a finite length of metamaterial. Using these data a retrieval procedure was applied to obtain the effective permittivity ϵ and permeability μ, under the assumption that the metamaterial can be treated as homogeneous. This procedure confirmed [18, 19] that a medium composed of SRRs and wires could indeed be characterized by effective ϵ and μ with negative real parts over a finite frequency band, and a refractive index also with a negative real part.

In this paper we present a systematic numerical study of the transmission properties of LHMs and SRRs. The transfer matrix method (TMM) and the Microwave Studio (MWS) code were used, as well as a retrieval procedure for the calculation of effective ϵ and μ parameters. The TMM enables us to find the transmission, the reflection and their phase, through relatively large (of many unit cells) periodic LH structures. To obtain greater accuracy as regards the shape of the structures (although under the restriction of smaller structures—one or few unit cells) we utilize the newly developed, commercially available MWS code, which is based on the finite integration technique with perfect boundary approximation.

The paper is organized as follows. In section 2 we present a detailed parametric study of the SRR. The dependence of the magnetic resonance frequency, $\omega_{\rm m}$, and of the electric resonance frequency, ω_0, on the SRR size for a single-ring SRR in the propagation direction is presented in section 2.2 and a comparison between circular and rectangular SRRs is given in section 2.3. Moreover, a comparison between the resonance frequencies of single-ring SRRs and that of double-ring SRRs is given in section 2.4 and, finally, in section 2.5 the dependence of $\omega_{\rm m}$ on the width and depth of the rings, on their separation, on the ring gap and on the background material is discussed. In section 3 we discuss the influence on the SRR transmission of the SRR orientation relative to the incident electric field and the issue of the electric coupling to the magnetic resonance. In section 4 we consider combined metamaterials of rectangular double-ring SRRs and wires and we present a detailed study of the dependence of the LH transmission on the dielectric constant of the substrate, on the distance between the wires and the SRRs, on the thickness of the unit cell and on the orientation of the SRRs relative to the wires. In section 5 we present results for the effective plasma frequency of the combined system of wires and closed SRRs. Section 6 deals with symmetric SRRs, which do not couple with the incident electric field, and therefore can be used in 2D and 3D isotropic metamaterial designs. Finally, in section 7 we present our conclusions.

2. Parametric study of SRR elements

2.1. Single-ring SRRs

In order to obtain a magnetic resonance which possesses a region with $\mu < 0$ it is not necessary to have a double-ring SRR, as was probably thought and mostly done so far both in the experiments and in the simulations. A single ring with a cut (a single-ring SRR) behaves also as a magnetic resonator. This is demonstrated in figure 1(a), where we plot the transmission as a function of frequency for a single-ring SRR, both for a circular and a square one, of the same linear dimension and metal and unit cell characteristics. Notice that both the circular and the square single-ring SRRs give a dip in the transmission coefficient (the first dip in figure 1(a)) which is associated with a negative μ regime (see panel (b)). The frequency of this dip, i.e. the magnetic resonance frequency, $\omega_{\rm m}$, is a little lower for the square SRR than for the circular one. The inductance in this single-ring resonator is provided by its circular or square metallic loop, while the capacitance is given by the gap (cut) of the ring. The second dip in the transmission of figure 1(a), at $\omega = \omega_0$ ($\approx$70 GHz for the tetragonal ring) corresponds to the electric cut-wire-like response of the SRR [10], i.e. to a resonance in its electrical permittivity, ϵ. Since the ring exhibits both a magnetic and an electric resonance (associated with a $\mu < 0$ and an $\epsilon < 0$ regime, respectively), theoretically it might be possible to achieve a LH transmission regime using only an array of SRRs (i.e. no additional continuous wires are needed to get the negative ϵ response), by tuning the magnetic resonance (at $\omega_{\rm m}$) into the negative ϵ band (at ω_0) provided by its own electric cut-wire response.

2.2. Controlling ω_m and ω_0 for one single-ring SRR

One of the aims in the studies of LHMs is to shift the magnetic resonance frequency, $\omega_{\rm m}$, below the cut-off frequency ($\omega_{\rm p}'$)

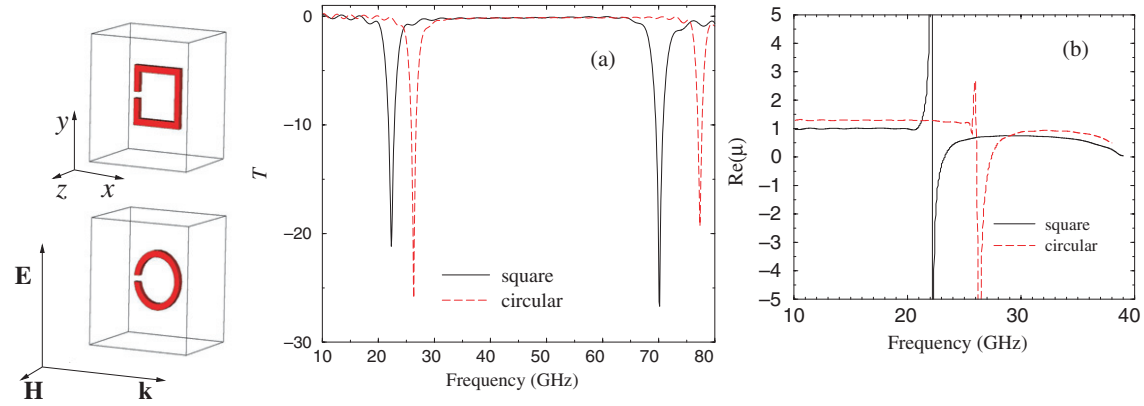

Figure 1. (a) Transmission (T, in dB) versus frequency for one single-ring square (solid curve) and a circular (dashed curve) SRR. The corresponding designs are shown on the left side of the panel. For the square SRR the ring width, depth and the gap all are 0.2 mm, and the linear SRR size is 1.8 mm. The SRR is placed in air, in a computational cell with dimensions $3.8 \times 3.8 \times 3.2$ mm^3, along x, y and z directions, respectively. The boundary conditions are $E_\parallel = 0$ at $y = 0$ and 3.8, and $H_\parallel = 0$ at $z = 0$ and 3.2 (at the boundaries of the computational cell). The circular SRR has outer diameter 1.8 mm and the computational cell and the materials characteristics are like those for the square one. The electric field (**E**) propagation direction and polarization are shown together with the SRR designs. (b) Magnetic permeability, $\mu(\omega)$, as a function of frequency for the single-ring square (solid curve) and circular (dashed curve) SRR, at frequencies around the magnetic resonance frequency.

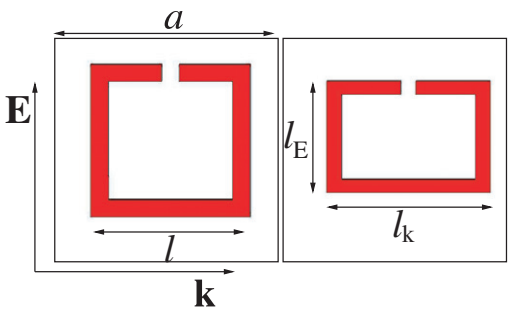

Figure 2. Two single-ring SRRs, a square one and an orthogonal one, are shown, together with the external electric field, **E**, polarization and propagation directions and the lattice constant, a, of the square unit cell. For the orthogonal SRR (with identical lattice, electric field polarization and propagation direction) the lengths, ℓ_k and ℓ_E, of the two sides of the orthogonal SRR are also shown.

of the electric response of the combined system of SRRs and wires, i.e. in the $\epsilon < 0$ regime. Since the cut-off frequency ω_p' depends strongly on the electric cut-wire response of the SRR (at ω_0; see [10] as well as section 5, below), the requirement $\omega_m < \omega_p'$ suggests that one has to be able to control both the magnetic and the electric SRR resonance frequencies, ω_m and ω_0 respectively. The first step towards this control is the understanding of the dependence of the ω_m and ω_0 on the various SRR parameters. Here we examine their dependence on the SRR size, and more specifically on the SRR area and side length (see figure 2). This study is done in a periodic arrangement of SRRs, using the transfer matrix method (the unit cell characteristics and the incident wave polarization and propagation direction are shown in figure 2).

The ω_m and ω_0 dependence on the SRR area for a square SRR is shown in figure 3(a). There, we plot ω_m and ω_0 as a function of a/ℓ, where ℓ is the side length of the SRR (see figure 2) and a is the size of the unit cell or the lattice constant at the SRR plane (see again figure 2). As can be seen from figure 3(a), for a single-ring square SRR, $\omega_m \propto 1/\ell$, i.e. ω_m^2 is inversely proportional to $1/\ell^2$, which is the SRR area.

Further studies (not presented here), including also non-square rings, showed that, in general, ω_m^2 is indeed inversely proportional to the ring area, in agreement with the well accepted formula $\omega_m^2 \sim 1/LC$. (Notice that the self-inductance, L, in this formula is approximately proportional[6] to the area of the SRR loop.) The electric resonance, ω_0, also increases as a/ℓ increases. However, its dependence is weaker than that of ω_m. The different dependences of ω_m and ω_0 on a/ℓ allows us to control the relative position of ω_m and ω_0, something that can be proved to be of great power in the study of left-handed materials.

Varying now the side of the SRR (ℓ_k in figure 2) which is perpendicular to the incident electric field direction and keeping ℓ_E constant, we also calculated ω_m and ω_0, The dependence of ω_m and ω_0 versus a/ℓ_k is shown in figure 3(b). From figures 3(a) and (b) it can be seen that ω_0, for a single-ring SRR, depends only on its side parallel to the electric field, following the approximate relation $\omega_0 \propto a/\sqrt{\ell_E}$, with a being the corresponding lattice constant. This is the reason that ω_0 is constant in figure 3(b), while $\omega_0 \propto a/\sqrt{\ell}$ in figure 3(a).

2.3. *Circular versus rectangular SRRs*

Comparing the transmission properties as well as the retrieval values of μ for circular and square single-ring SRRs (see figure 1) we find no qualitative difference between the two cases. For circular and square single-ring SRRs with the same linear dimension, metal characteristics and gaps, the circular SRR shows, in general, higher values of ω_m and ω_0, in agreement with what was discussed in the previous section 2.2 (due to the smaller area and the smaller 'side length'). Nevertheless, the ω_m and ω_0 dependence on the system parameters is the same in both cases. Therefore, in the following we will restrict ourselves to exclusively square SRRs, due to the simplicity of the corresponding calculation.

[6] For a solenoid the self-inductance is proportional to the area; for a single circular ring of radius r with circular cross-section of radius b the self-inductance is $4\pi r[\ln(8r/b) - 7/4]$. The present case because of the boundary conditions is in between.

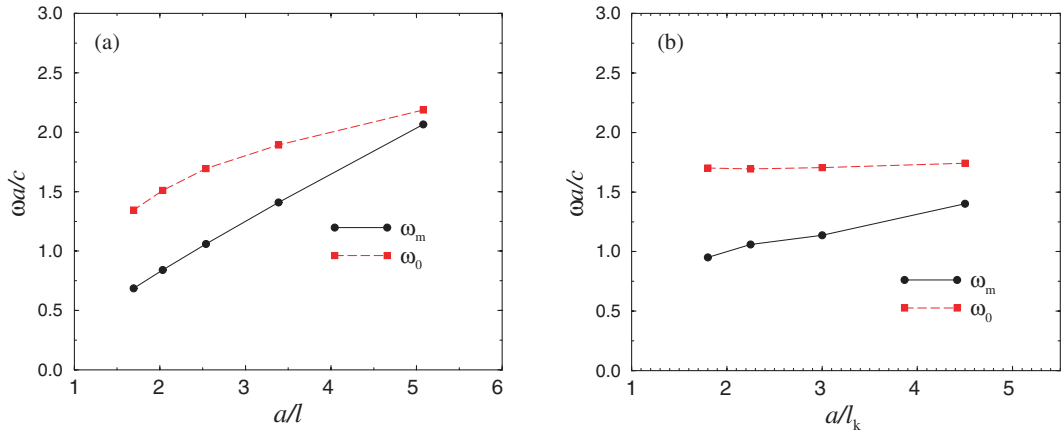

Figure 3. (a) ω_m and ω_0 (in units of c/a, where c is the vacuum light velocity and a is the lattice constant of the square unit cell) versus a/ℓ for a square single-ring SRR like the one shown in the left panel of figure 2. ℓ is the SRR side length. (b) ω_m and ω_0 (in units of c/a) versus a/ℓ_k for an orthogonal single-ring SRR (see figure 2, right panel). ℓ_k is the length of the SRR side which is perpendicular to the incident electric field, **E**.

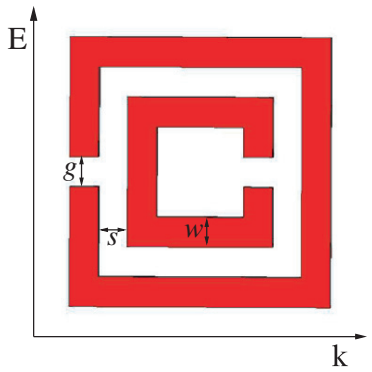

Figure 4. Our model double-ring SRR. $g = s = w = 0.2$ mm; metal depth = 0.2 mm. The SRR side is 1.8 mm. The computational cell and the boundary conditions used in the calculations are the same as those described under figure 1.

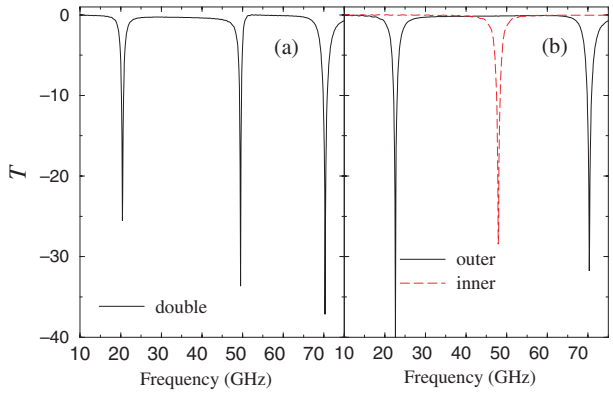

Figure 5. Transmission (T, in dB) versus frequency (in GHz) for the double-ring SRR shown in figure 4(a), and for its isolated outer and inner ring SRRs (b). The background material is air.

2.4. Single- versus double-ring SRRs

Since a single ring acts also as a magnetic resonator, providing a negative μ regime, what are the benefits from the addition of a second ring and why so far, in almost all of the existing experimental efforts, is the double-ring SRR the preferable building block? To compare the two cases (double- versus single-ring SRRs) we use the model SRR presented in figure 4.

In figure 5(a) we present the transmission through the double-ring SRR of figure 4 and in figure 5(b) the transmission through only its outer or its inner ring SRR. (The electromagnetic (EM) field propagation and polarization are as shown in figure 4. The transmission has been calculated using MWS and considering only one SRR in the propagation direction.) Comparing figures 5(a) and (b), it can be seen that the lower magnetic resonance frequency of the double ring (see the first dip in figure 5(a)) is essentially that of the outer ring, but with a relatively small downwards shift. This shift is due to the additional capacitance between the rings. Detailed studies of the field and current distribution showed that in the double-ring case the currents at the first resonance move in the same direction in both rings, having as a result opposite charges at the facing sides of the outer and inner ring; thus a capacitor is formed between the rings and its capacitance is added to that given by the gap of the outer ring; the result is the lowering of the resonance frequency with respect to that of just the outer ring.

The second dip of the double-ring case corresponds essentially to the magnetic resonance of the inner ring, with a small upwards shift (there, the currents in the two rings of the SRR move in opposite directions). The strength of this resonance is sometimes very small, showing that the magnetic response of the inner ring is screened by the presence of the outer one. This happens mainly in the cases where the electric field is parallel to the continuous sides of the SRR.

Another important characteristic of the double ring is that it contains in its spectrum also the electric responses of its two component rings; see, e.g., the third dip of figure 5(a), which corresponds to the electric cut-wire response of the outer ring (of its longer side).

One advantage of the double-ring SRR, compared with its outer single-ring resonator, as can be seen from figure 5, is that the magnetic resonance frequency of the double ring occurs at a relatively lower frequency; thus there is a higher probability for the magnetic response to lie in the $\epsilon < 0$ regime of the combined system of SRRs and wires. Another advantage

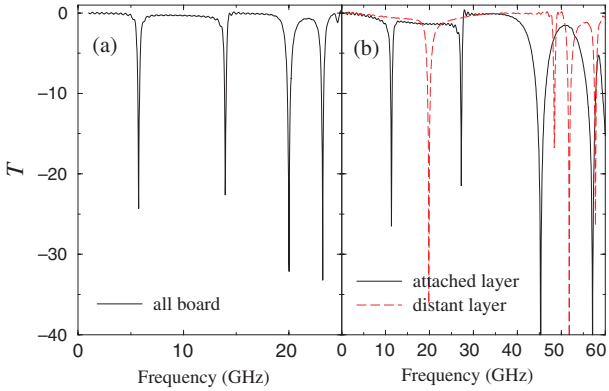

Figure 6. (a) Transmission (T), in dB, as a function of frequency for the resonator of figure 4. The background material has a dielectric constant $\epsilon_b = 12.3$. (b) T versus frequency for the resonator of figure 4, but the background material is composed of air plus a slab of dielectric, of $\epsilon = 12.3$ and dimensions $3.8 \times 3.8 \times 0.2$ mm^3 (3.8×3.8 is the size at the SRR plane). The solid curve shows the T if the SRR is attached on the dielectric slab and the dashed curve shows the T if the SRR is 0.2 mm away from the slab.

of the double-ring SRR appears when we put the rings in a periodic arrangement: the array of double-ring SRRs possesses a stronger magnetic resonance, which might lead to a more robust LH peak for the combined system of SRRs and wires.

2.5. The dependence of ω_m on the system parameters for a double-ring SRR

Continuing the efforts to understand the behaviour of the magnetic resonance frequency, ω_m, of a double-ring SRR, we examine next its dependence on various of the system parameters. More specifically, we examine how ω_m depends on the dielectric constant of the board, on the width, separation and depth of the rings, as well as on the gaps (cuts) of the rings. As a model system for this study we use the SRR presented in figure 4.

2.5.1. The influence of the board dielectric constant. In figure 6(a) we show the transmission (T) as a function of frequency for the resonator described in figure 4, embedded inside a background (board) material with dielectric constant $\epsilon_b = 12.3$ (corresponding to GaAs). The T for $\epsilon_b = 1$ is shown in figure 5(a). Comparing figure 6(a) with figure 5(a), it can be seen that as a result of the increase of the dielectric constant of the background there are reductions of both the electric and the magnetic resonance frequencies of the SRR. Detailed quantitative analysis showed that the dependence of ω_m on ϵ_b is of the form $\omega_m^2 \propto 1/\epsilon_b$.

The interesting point here is that ω_m depends not on the average ϵ_b in the unit cell but on the local values of ϵ_b nearby the SRR, and especially close to the gaps of the rings (although we are in the low frequency regime, where average values should be adequate for representing any spatially modulated dielectric properties of the board). This is demonstrated in figure 6(b), where we show the T for the case where the background material consists of a thin GaAs slab and the rest is air (the GaAs slab covers only 6.25% of the unit cell—its thickness is 0.2 mm). The solid curve in figure 6(b) shows the T when

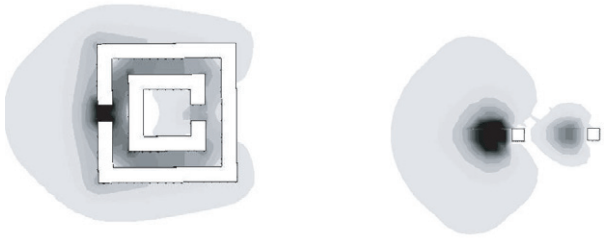

Figure 7. The electric field intensity (E^2) for the SRR of figure 4, at the magnetic resonance frequency. The left panel shows the field at the SRR plane and the right panel the field at a plane perpendicular to that of the SRR, which passes through the SRR gaps.

the SRR is printed on the GaAs slab and the dashed curve that when the SRR is moved 0.2 mm away from this slab. Neither of the two cases can be deduced from figure 5(a) using the relation $\omega_m^2 \propto 1/\bar{\epsilon}_b$, with $\bar{\epsilon}_b$ an average value.

The fact that the same amount of dielectric in the unit cell affects the transmission differently, depending on its position, can be understood if one takes into account the strong inhomogeneity and the local spatial character of the field in the system, especially at the resonance frequencies. At the magnetic resonance, the electric field has its maximum mainly at the SRR outer ring gap and in the region between the rings, while along the direction perpendicular to the SRR plane it is not very much extended (see figure 7). Taking into account this form of the field as well as the strong influence of the dielectric constant on the capacitance, it is not difficult to understand the different influences of the dielectric at the different positions of the unit cell.

Another interesting thing to note here is that on changing the dielectric constant of the total background material the T spectrum is moved to different frequencies but its form remains unchanged, i.e. all the characteristic frequencies depend in the same way on the background dielectric constant. This is not the case if the background material is not homogeneous.

2.5.2. The influence of the width, separation and depth of the rings. Since the capacitance between the rings, which depends on the ring separation, is a component of the total capacitance of the SRR, one expects the magnetic resonance frequency to depend also on the ring separation, s. This dependence is shown in figure 8(a): reduction of s results in a decrease of the magnetic resonance frequency (see the shift of the first T dip in figure 8(a)). This is expected, as reduction of s is equivalent to increase of the inter-ring capacitance (note that $\omega_m \propto 1/\sqrt{LC}$ and for a parallel plane capacitor with separation of plates s, $C \propto 1/s$). From figure 8(a) it can be seen that a 50% reduction of s results in an almost 13% downshift in ω_m.

In figure 8(b) we show how the transmission is affected by the ring width (w), as well as the combined influence of the changing of both the width and separation of the rings. Ring width affects the inductance, L, of the loops: smaller width means larger inductance (see footnote 5) and thus smaller ω_m. Figure 8(b) indicates that a 50% reduction of w results in an almost 15% downshift of ω_m.

Changing both the ring separation and their width, the shift in ω_m of the first resonance is approximately the sum of the two shifts coming from the separate changes of w and s.

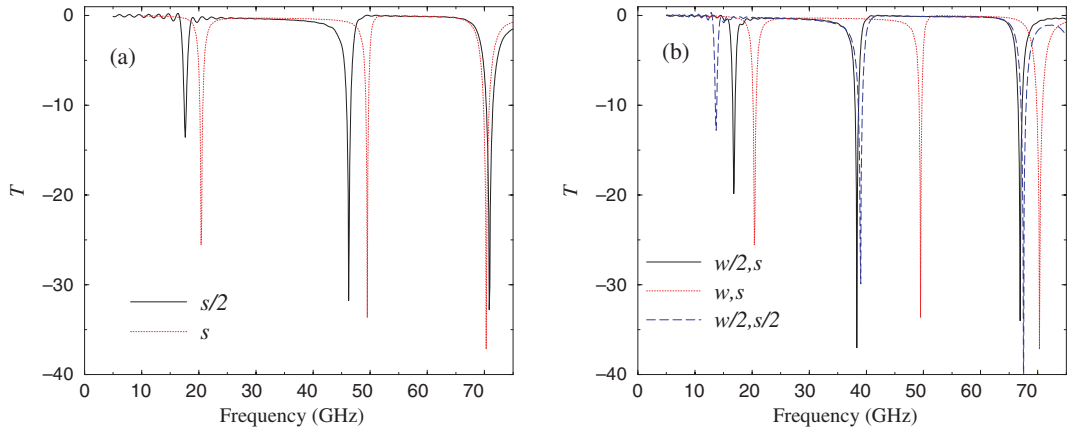

Figure 8. (a) Transmission (T), in dB, versus frequency for the SRR of figure 4 (dotted curve), where $s = 0.2$ mm, and with an SRR arising from that of figure 4 by reducing s to 0.1 mm (increasing the inner ring size). The background material is air. (b) The dotted curve is the same transmission as in (a) ($s = 0.2$ mm, $w = 0.2$ mm), the solid curve shows the T for ring width $w = 0.1$ mm and separation $s = 0.2$ mm and the dashed curve the T for $s = w = 0.1$ mm.

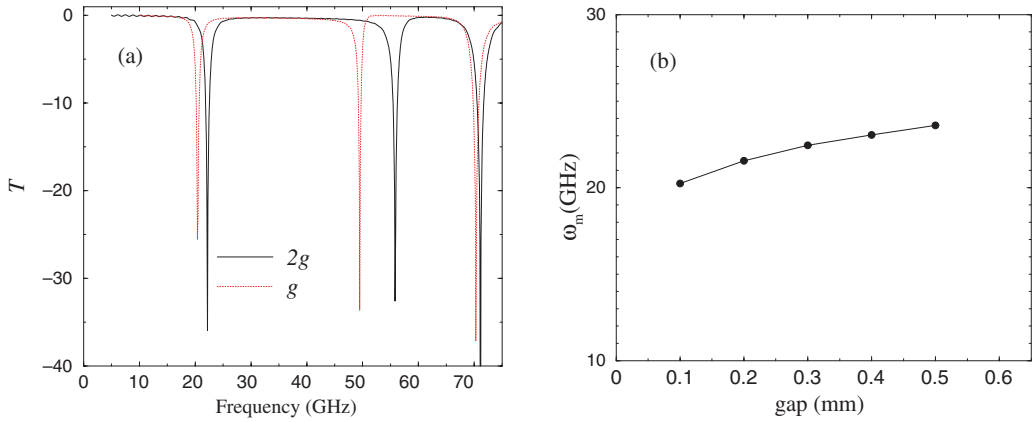

Figure 9. (a) Transmission coefficient (T), in dB, versus frequency for the SRR of figure 4 (dotted curve; SRR gap size $g = 0.2$ mm) and for the same type of SRR but with gap size $g = 0.4$ mm (solid curve). (b) The dependence of the magnetic resonance frequency, ω_m, on the size of the SRR gaps is shown. The background material is everywhere air.

Something worth noticing here is that in all the cases of figure 8 where downshift of ω_m takes place, this shift is accompanied by a reduction of the strength of the resonance. Thus, although the desired condition is for ω_m to be as low as possible, one has to pay special attention that the lowering of ω_m is not associated with a weakening of the magnetic response of the SRR.

As regards the influence of the depth of the rings on the magnetic resonance frequency, it seems that this is insignificant provided that the depth of the rings is a few times larger than the skin depth of the metal at the frequency regime of interest.

2.5.3. The influence of the gaps (cuts) of the rings. The influence of the size (g) of the gaps of the rings is illustrated in figure 9. On reducing the gap size, ω_m is reduced. The influence of the gap size in ω_m seems, though, to be smaller than the influence of the ring separation.

3. SRR orientation relative to the electromagnetic field: second electric coupling

For the SRR orientation in one-dimensional (1D) LH materials there are two possibilities: either the one shown in figure 4, i.e. the electric field, **E**, parallel to the SRR sides bearing the cuts, or its 90° rotated case, i.e. **E** perpendicular to these sides. These two geometries are those marked (B) and (A) in the left panel of figure 10.

The transmission for these two geometries as a function of frequency is shown in the right panel of figure 10 (for the calculation method and the computational cell see also figure 1). What can be seen there is that the lower magnetic resonance frequencies of the SRR are almost the same in the two orientations. What is changed is the frequency of the electric cut-wire response (see the third dip of each curve), which is higher for the geometry (B).

Examining periodic systems of SRRs, where due to the interactions among the SRRs the transmission dips become broader, we found that the T dip corresponding to the magnetic resonance frequency is broader and deeper for the geometry (B). This broader dip, though, was not associated with a broader LH peak when we combined the SRRs with wires. The LH peak for the case (B) was rather narrower and weaker, a result that was initially very puzzling. The issue was resolved in the attempts to study two-dimensional (2D) and three-dimensional (3D) materials, where for the orientation of the SRR relative to the EM field two additional possibilities are

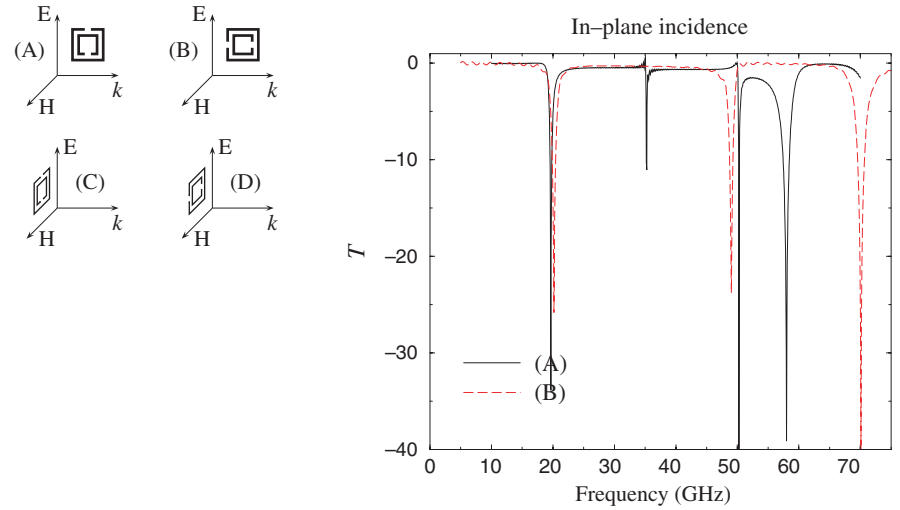

Figure 10. Left panel: the four possible orientations of the SRR relative to the electromagnetic (EM) field propagation direction and polarization. Right panel: transmission coefficient (T, in dB) versus frequency for an SRR with the parameters those of figure 4, oriented with respect to the EM field as in configuration (A) (solid curve) and as in (B) (dashed curve). (A) and (B) are shown in the left panel.

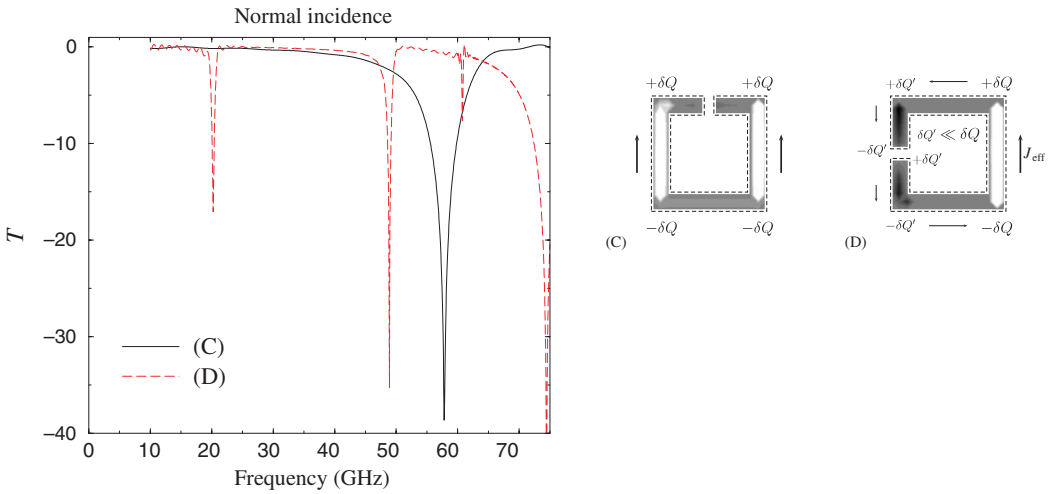

Figure 11. Left panel: transmission coefficient (T, in dB) versus frequency for an SRR with the parameters those of figure 4, oriented with respect to the EM field as in configurations (C) (solid curve) and (D) (dashed curve), of figure 10, left panel. Right panel: plots showing the component of the current density, **J**, parallel to the electric field for a single-ring SRR oriented as in configurations (C) (left plot) and (D) (right plot) of figure 10, left panel, at the magnetic resonance frequency. White indicates positive values and black negative. δQ means the charge. The external electric field points upwards. Only in the case of broken symmetry, (D), will a circular current appear which excites the magnetic resonance of the SRR.

involved, those marked (C) and (D) in figure 10. These two orientations should be magnetically inactive, as the incident magnetic field is in the plane of the SRR, and thus unable to excite resonant circulating currents around the SRR rings.

Surprisingly, studying the orientation (D), we found [21] a dip at the magnetic response frequency of the SRR (see figure 11). Similar results were obtained also by Gay-Balmaz *et al* [22]. This dip is again due to resonant currents circulating around SRR rings. How are these circulating currents excited, since it cannot be through the external magnetic field? What we found is that they are excited through the external electric field. The possibility of coupling with the electric field is given by the asymmetry of the SRR with respect to this electric field. The case is illustrated in the right panel of figure 11, where we show the component of the current density parallel to **E**, at the magnetic resonance frequency, for a single-ring SRR oriented with respect to the EM field as shown in configurations (C) and (D) of figure 10, left panel.

As shown in figure 11, for the configuration (D), the asymmetry of the SRR with respect to the external **E** leads to a charge distribution asymmetry, which is compensated through a circular current. Thus, not only the magnetic field but also the electric field of the incoming wave can couple to the resonance of the circulating currents in the SRR. The most important effect of this coupling, which will be called here second electric coupling (to be distinguished from the electric coupling through the cut-wire-like resonance, at ω_0), is an electric resonant response (a resonance in ϵ) around the SRR magnetic response frequency, ω_m. Detailed studies showed that this electric response, which comes from the non-zero average electric polarization of the (asymmetric) SRR, occurs in fact at a frequency slightly shifted from ω_m (slightly above

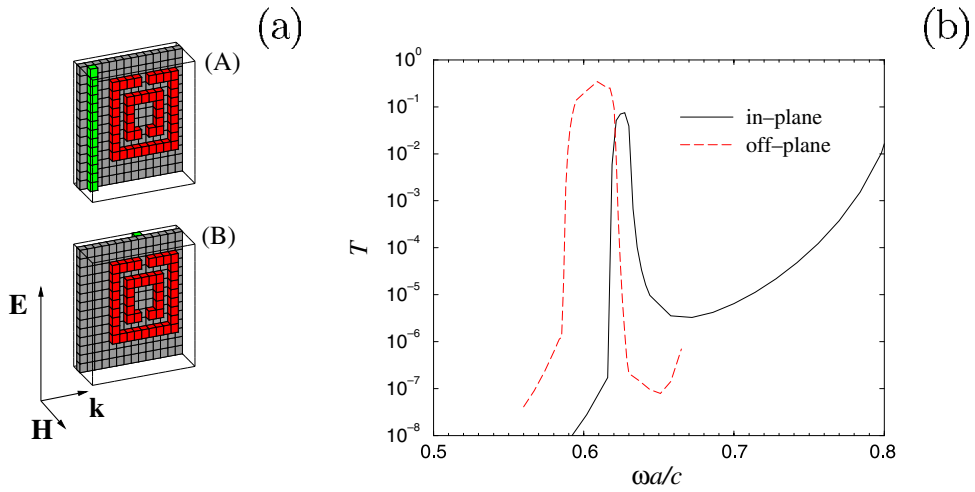

Figure 12. (b) Transmission coefficient (T, in dB) versus dimensionless frequency for the structures shown in the left panel, (a). The solid curve shows the T for configuration (A), i.e. wires next to the SRRs, and the dashed curve that for configuration (B), i.e. wires at the back of the board. The board is a thin dielectric layer (depth $= a/14$) of dielectric constant $\epsilon_b = 12.3$. The rest of the background material is air. The unit cell is a cube, with lattice constant a; the SRR has outer side length $9a/14$ and its other characteristic lengths are $a/14$. The wire has a cross-section at the **H**–**k** plane of $(a/14) \times (a/14)$.

ω_m in most of the cases studied). A possible result of this resonant ϵ is the addition of a right-handed transmission peak close to ω_m when the SRRs are combined with wires, which peak may diminish or even destroy the LH behaviour.

Another thing to note here is that the asymmetry as a result of which we have the second electric coupling is present also in the configuration (B) of figure 10. This might be the reason for the broader—than that of (A)—magnetic dip in the periodic SRR system, which is not associated with a broader LH peak of the combined system of SRRs and wires.

The problem of the asymmetry-mediated electric coupling will be present in all higher dimensional LHMs apart from some special cases which only work for a particular orientation or a constrained direction of propagation. The most secure solution of the problem is the invention and employment of more symmetric SRR designs (see section 6).

4. Parametric studies of LH materials

Using model systems with parameters close to those of LH structures which can be or have been constructed experimentally, we attempted a parametric study of LH materials, the results of which are presented in this section. Throughout this study we examined the influence on the LH regime (on the LH transmission window and the maximum transmitted power) of the following parameters:

(i) the board dielectric constant, ϵ_b;
(ii) the position of the wires relative to the SRRs;
(iii) the thickness of the unit cell; and
(iv) the loss parameter of the boards, ϵ_b''.

The aim of this study (which has been performed using the TMM) is to give the optimum parameters for obtaining a true broad LH transmission band with large transmitted power. This effort will offer a valuable way of designing the next generation of LHM experiments.

In what follows we consider structures with tetragonal, double-ring SRRs and continuous wires, patterned on thin dielectric boards which are separated by air. Below we briefly report on the main results.

4.1. The influence of the board dielectric constant

Systematic TMM studies concerning the dependence of the LH peak on the dielectric constant of the board, ϵ_b, showed that ϵ_b influences only the position of the LH peak, leaving its height and width almost unaffected (for lossless boards). The dependence of the LH peak position on ϵ_b follows the dependence of the magnetic resonance, discussed in the previous section 2.5: on increasing ϵ_b the LH peak is moved to lower frequencies, with the peak frequency inversely proportional to the square root of ϵ_b.

4.2. The influence of the position of the wires relative to the SRRs

For examining the influence of the relative SRR wires position we considered wires parallel to the imaginary line connecting the cuts of the SRR rings and we examined the configurations shown in figure 12(a). We found that the optimum position of the wires is that of configuration (B) of figure 12(a), i.e. the wires attached at the back of the dielectric boards, just behind the cuts of the rings. Configuration (A), although it is easier to fabricate experimentally [6], gives a narrower and somehow lower LH peak (see figure 12(b)). Thus, configuration (B) is the best structure for robust LH transmission.

Trying to examine the effect of moving the wire parallel to itself along the **H** direction for the configuration (B), we found that for cubic unit cells the distance of the wire from the resonator plane does not influence the LH peak very much.

4.3. The influence of the unit cell thickness (the lattice constant along the direction perpendicular to the SRR plane)

In figure 13 we show the evolution of the LH transmission peak of figure 12(b), configuration (B), as one changes the unit cell thickness, a_H (i.e. the distance of two successive SRR + wire planes along the **H** direction (see figure 12(a))). One can see

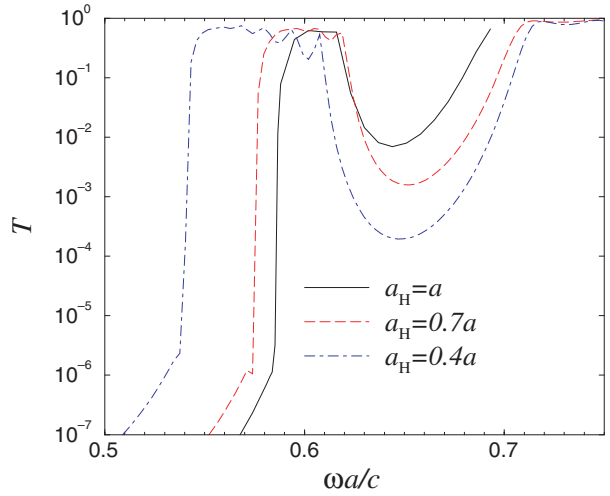

Figure 13. Transmission coefficient (T, in dB) versus dimensionless frequency for the geometry (B) of figure 12, for three different unit cell sizes, $a_{\rm H}$, in the direction perpendicular to the SRR plane. The other parameters are those mentioned in figure 12. $a = a_{\rm E} = a_{\rm k}$ is the lattice constant (unit cell size) in the plane of the SRR.

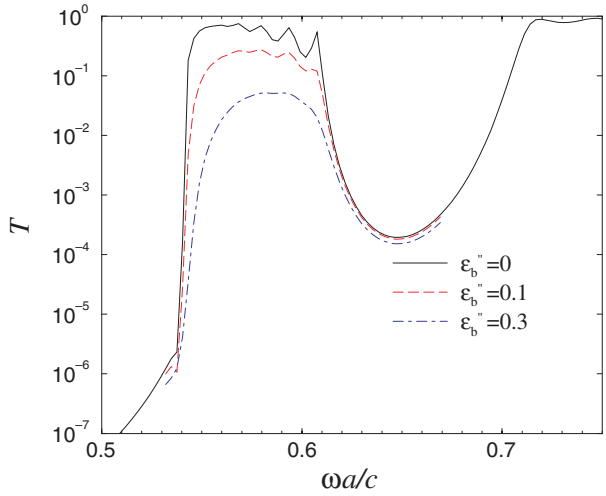

Figure 14. The evolution of the transmission coefficient (T, in dB) of figure 13, dotted–dashed curve, as one adds to the dielectric constant of the board an imaginary part, $\epsilon_{\rm b}''$. The horizontal axis is a dimensionless frequency, normalized with the unit cell size at the SRR plane, a, and with the vacuum light velocity, c.

that as the successive SRR + wire planes come closer, the LH peak becomes much broader. The reason is the broadening of the negative μ regime due to the increasing amplitude of the magnetic resonance of the approaching SRRs, i.e. due to the stronger interaction among the SRR magnetic resonances. Moreover, as a result of the reduction of the unit cell size in the continuous wire lattice there is an increase of the cut-off (plasma) frequency, $\omega_{\rm p}$, of the wires and thus an increase of the cut-off frequency, $\omega_{\rm p}'$, of the combined SRRs + wires system (see also section 5). Thus the LH peaks become more clearly resolved and separated from the neighbouring right-handed T shoulders.

4.4. The influence of the loss parameter (conductivity or ϵ_b'') of the dielectric boards

The $\epsilon_{\rm b}''$ (imaginary part of the dielectric constant) of the boards was proved to be one of the most critical parameters [12, 13, 15] for the left-handed transmission window. An example of its influence is shown in figure 14. One can see that even small $\epsilon_{\rm b}''$ values can lead to a very large T reduction. This parameter is critical even if the dielectric boards are very thin, since, especially for high index boards, there is a high concentration of field inside the boards.

5. The combined metamaterial electric cut-off frequency, ω_p'

It was recently recognized [10] that the electric response of the LHMs is not due only to the electric response of the metallic wires; it is also strongly affected by the electric response of the SRRs. The SRRs respond electrically like a system of cut wires, exhibiting a resonance at a frequency ω_0. (This response can be demonstrated by closing the SRRs, destroying thus their magnetic response.)

As a result of the presence of the SRRs, the electric cut-off frequency, $\omega_{\rm p}'$, of the combined system of wires and SRRs (or closed SRRs) is always lower [11, 20] than the cut-off (plasma) frequency of the continuous wires alone ($\omega_{\rm p}$). The role of the SRRs in the formation of the electric response of the combined system of SRRs and wires is illustrated in figure 15.

Below, we discuss the dependence of the cut-off frequency $\omega_{\rm p}'$ on (i) the depth and width of the continuous wires, (ii) the depth and width of the SRR rings.

5.1. The influence of the depth and width of the continuous wires

From the above discussion and from figure 15 it becomes clear that $\omega_{\rm p}'$ can be increased through increase of $\omega_{\rm p}$ of the continuous wires, although it would remain lower than ω_0. Our studies showed that $\omega_{\rm p}$ of the wires increases as the width of the metallic wires increases. Calculations of the transmission coefficient through the combined system of closed SRRs and wires showed that $\omega_{\rm p}'$ also increases as the width of the metallic wires increases, but the increase depends also on the relative position and distance of $\omega_{\rm p}$ and ω_0.

The *depth* of the wires has an effect similar to that of the width on $\omega_{\rm p}$: increasing the depth leads to increase of both $\omega_{\rm p}$ and $\omega_{\rm p}'$.

5.2. The influence of the depth and width of the SRR rings

Detailed transmission studies showed that the width of the SRR rings has almost no effect on $\omega_{\rm p}'$. The same is true also for the SRR depth. This is of great importance as the depth and width of the SRRs have considerable effects on $\omega_{\rm m}$. Thus, since $\omega_{\rm m}$ is controlled only by the SRRs while $\omega_{\rm p}'$ is controlled also by the wires, one has the *ability to control the electric and magnetic responses of the LHMs independently*.

6. Symmetric SRR structures

The general problem with the rings of only one gap (cut) in the SRR designs considered so far is the inherent asymmetry of the

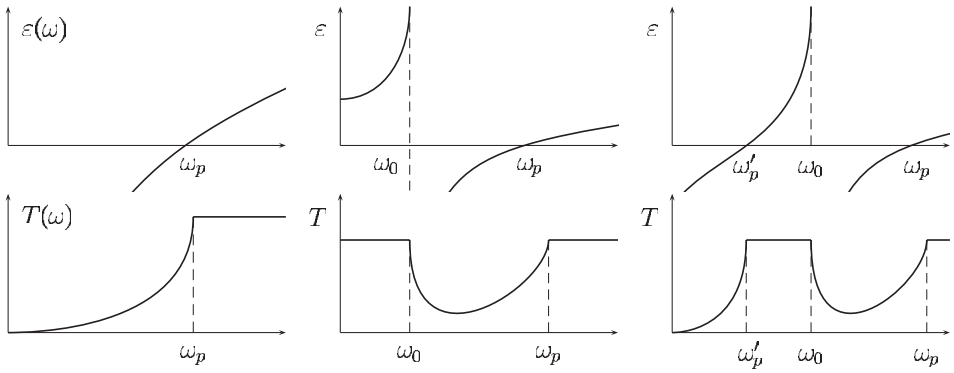

Figure 15. An illustration of the electric response to an incident EM field of a system of continuous wires (left panels), of cut wires (or SRRs or closed SRRs) (middle panels) and of the metamaterials of wires plus cut wires or SRRs (right panels). Both the electrical permittivity ϵ (top panels) and the resulting transmission coefficient T (bottom panels) as a function of frequency are shown, and the characteristic frequencies, ω_p, ω_0 and ω'_p, of these systems are marked. It is shown that the combination of a system of continuous wires with a system of cut wires (or SRRs) results in a spectrum with remarkable differences compared to that for the system of continuous wires only.

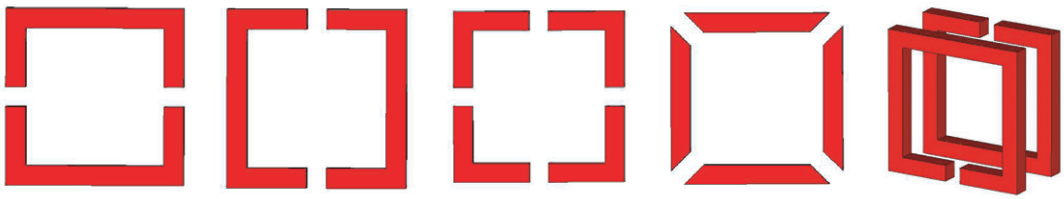

Figure 16. Five SRR designs, more symmetric than the conventional and most commonly used SRR presented in figure 4. The advantage of these symmetrized SRRs is the avoidance of the second electric coupling, described in section 3. The disadvantage is the higher magnetic resonance frequency, due to the many gaps (cuts).

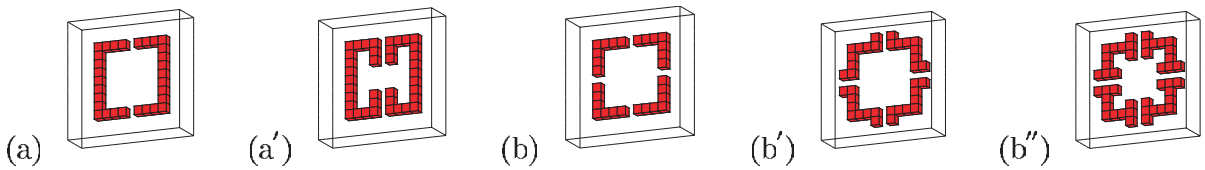

Figure 17. Modifications, (a′) and (b′), (b″), of two of the SRR designs presented in figure 16. These modifications result in lower magnetic resonance frequency compared with their original SRRs, (a) and (b).

resulting SRRs. As discussed in section 3, this will lead to the occurrence of the electric coupling to and response from the magnetic resonances (second electric coupling) [21]. This is an unwanted feature for fabricating higher dimensional systems. Marques *et al* considered bianisotropy in SRR structures and developed an analytical model for evaluating the magnitude of cross-polarization effects [23].

To avoid this second electric coupling, more symmetric SRRs should be used. The idea in the design of more symmetric SRRs is to keep the inductance provided by the loop of the SRR ring but to distribute the capacitance of the single gap to two or four gaps, symmetrically around the ring, as shown in figure 16. This will lift the asymmetry of the SRR plane and therefore eliminate the second electric coupling.

The problem arising in this kind of design is the difficulty of maintaining the capacitance of the single-gap ring, as the gaps act like capacitors in series, leading to a considerable lowering of the total capacitance and thus to an increase of ω_m. (The magnetic frequency for a ring with n gaps equal in size goes as $\omega_m^2(n \text{ gaps}) \sim n\omega_m^2(1 \text{ gap})$.) This a disadvantage of the design as it decreases the probability of ω_m lying below the cut-off frequency of the electric response of the system.

One solution to the problem could be a decrease in the size of the gaps, although this, in many cases, is limited by technology. Another solution could be a modification in the designs, with the capacitance of the gaps being increased. Such modifications for two of the structures of figure 16 are shown in figure 17. The result from such a modification is usually a lowering of ω_m but not always an improvement in the transmission picture, as the strength of the magnetic resonance and the width of the $\mu < 0$ regime are affected as well.

In figure 18 we show four of the most promising SRR designs which emerged from the above-mentioned study on more symmetric SRRs and which are currently under further investigation.

7. Conclusions

We systematically studied the magnetic and the electric response of single-ring and double-ring SRRs, both circular and rectangular. The dependence of the magnetic resonance frequency, ω_m, and of the electric resonance frequency, ω_0, of the SRR on the length, width and depth of the metallic sides for different kinds (circular or square, single- or double-ring)

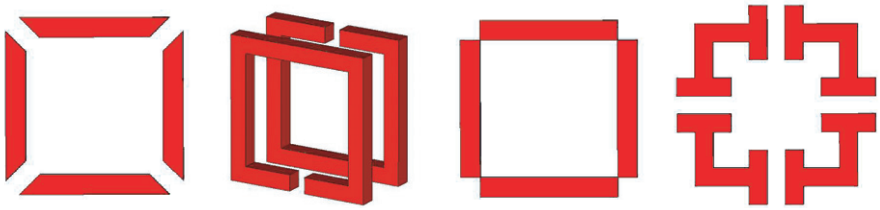

Figure 18. Four of the most promising 'symmetric' SRR designs.

of SRRs was examined. It was found that both ω_m and ω_0 for circular and rectangular SRRs are essentially the same and therefore most of our studies were done for rectangular SRRs because of the simplicity of the corresponding transmission calculations.

We also studied the transmission characteristics of LH structures composed of square SRRs and wires. The dependence of the LH transmission peak on the real (ϵ_b) and imaginary (ϵ_b'') parts of the dielectric constant of the dielectric boards was examined. ϵ_b'' was proved to be one of the most critical parameters for the LH transmission, as even a small change of it can lead to a very large reduction of the LH transmission peak.

Among the possible configurations of SRRs and wires that we examined, the best for producing the most robust LH transmission peak was found to be the one that has square SRRs on one side of the dielectric board and wires on the other side of the board, just behind the cuts of the rings of the SRRs. The dependence of the LH transmission peak on the unit cell thickness and on the distance between the SRRs and the wires for this configuration were also examined.

Another thing that we also studied is the role of the SRR orientation relative to the incident EM field and the resulting issue of the electric coupling to the magnetic resonance, i.e. the coupling of the external electric field to the resonance of the currents circulating around SRRs. This coupling, which represents an unwanted feature as it is associated with a resonance in the electric response of the system, is a result of lack of symmetry and will always be present in 2D and 3D LH structures composed of non-symmetric SRRs. In the attempts to avoid this coupling we investigated highly symmetric SRR structures and their behaviour in 2D and 3D LH media. We identified some optimum designs, which may constitute components of promising 2D and 3D LH structures.

Our detailed numerical results on SRRs and left-handed materials (consisting of SRRs and wires) will help in the theoretical understanding, analysis, development, fabrication and testing of LHMs, and possibly help in the investigation of the feasibility of their use in different applications.

Acknowledgments

Financial support from EU_FET project DALHM, NSF (US–Greece Collaboration), and DARPA (Contract No MDA972-01-2-0016) is acknowledged. This work was partially supported by Ames Laboratory (Contract No W-7405-Eng-82).

References

[1] Veselago V G 1967 *Usp. Fiz. Nauk* **92** 517
Veselago V G 1968 *Sov. Phys.—Usp.* **10** 509 (Engl. Transl.)
[2] Pendry J B, Holden A J, Stewart W J and Youngs I 1996 *Phys. Rev. Lett.* **76** 4773
Pendry J B, Holden A J, Stewart W J and Youngs I 1998 *J. Phys.: Condens. Matter* **10** 4785
[3] Pendry J B, Holden A J, Robbins D J and Stewart W J 1999 *IEEE Trans. Microw. Theory Tech.* **47** 2057
[4] Pendry J B 2000 *Phys. Rev. Lett.* **85** 3966
[5] Smith D R, Padilla W J, Vier D C, Nemat-Nasser S C and Schultz S 2002 *Phys. Rev. Lett.* **84** 4184
[6] Shelby R A, Smith D R, Nemat-Nasser S C and Schultz S 2001 *Appl. Phys. Lett.* **78** 489
Bayindir M, Aydin K, Ozbay E, Markoš P and Soukoulis C M 2002 *Appl. Phys. Lett.* **81** 120
[7] Li K, McLean S J, Gregor R B, Parazzoli C G and Tanielian M 2003 *Appl. Phys. Lett.* **82** 2535
[8] Shelby R A, Smith D R and Schultz S 2001 *Science* **292** 77
[9] Parazzoli C G, Gregor R, Li K, Koltenbach B E C and Tanielian M 2003 *Phys. Rev. Lett.* **90** 107401
Houck A A, Brock J B and Chuang I L 2003 *Phys. Rev. Lett.* **90** 137401
[10] Koschny T, Kafesaki M, Economou E N and Soukoulis C M 2004 *Phys. Rev. Lett.* **93** 107402
[11] Katsarakis N, Koschny T, Kafesaki M, Economou E N, Ozbay E and Soukoulis C M 2004 *Phys. Rev.* B **70** 201101
[12] Weiland T, Schummann R, Greegor R B, Parazzoli C G, Vetter A M, Smith D R, Vier D V and Schultz S 2001 *J. Appl. Phys.* **90** 5419
Markoš P and Soukoulis C M 2002 *Phys. Rev.* E **65** 036622
[13] Markoš P, Rousochatzakis I and Soukoulis C M 2002 *Phys. Rev.* E **66** 045601
[14] Pacheco J, Grzegorczyk T M, Wu B-I, Zhang Y and Kong J A 2002 *Phys. Rev. Lett.* **89** 257401
[15] Markoš P and Soukoulis C M 2003 *Opt. Express* **11** 649
Markos P and Soukoulis C M 2003 *Opt. Lett.* **28** 846
[16] O'Brien S and Pendry J B 2002 *J. Phys.: Condens. Matter* **14** 4035
O'Brien S and Pendry J B 2002 *J. Phys.: Condens. Matter* **14** 6383
[17] O'Brien S *et al* 2004 *Phys. Rev.* B **69** 241101
[18] Smith D R, Schultz S, Markoš P and Soukoulis C M 2002 *Phys. Rev.* B **65** 195104
[19] Koschny T, Markoš P, Smith D R and Soukoulis C M 2003 *Phys. Rev.* E **68** 065602
[20] Aydin K, Guven K, Zhang L, Kafesaki M, Soukoulis C M and Ozbay E 2004 *Opt. Lett.* submitted
[21] Katsarakis N, Koschny T, Kafesaki M, Economou E N and Soukoulis C M 2004 *Appl. Phys. Lett.* **84** 2943
[22] Gay-Balmaz P and Martin O J F 2002 *J. Appl. Phys.* **92** 2929
[23] Marques R, Medina F and Rafii-El-Idrissi R 2002 *Phys. Rev.* B **65** 144440